Close-Proximity Detection for Hand Approaching Using Backscatter Communication

Han Ding, Chen Qian, *Member, IEEE*, Jinsong Han, *Senior Member, IEEE*, Jian Xiao, Xingjun Zhang, *Member, IEEE*, Ge Wang, *Student Member, IEEE*, Wei Xi, *Member, IEEE*, and Jizhong Zhao, *Member, IEEE*

Abstract—Smart environments and security systems require automatic detection of human behaviors including approaching to or departing from an object. Existing human motion detection systems usually require human beings to carry special devices, which limits their applications. In this paper, we present a system called APID to detect hand approaching behaviors by analyzing backscatter communication signals from a passive RFID tag on the object. APID does not require human beings to carry any device. The idea is based on the influence of hand movements to the vibration of backscattered tag signals. APID is compatible with commodity off-the-shelf devices and the EPCglobal Class-1 Generation-2 protocol. In APID, a commercial RFID reader continuously queries tags through emitting RF signals and tags simply respond with their IDs. A USRP monitor passively analyzes the communication signals and reports the approach and departure behaviors. We have implemented the APID system for both single-object and multi-object scenarios. Extensive evaluations demonstrate that APID can achieve high detection accuracy in both scenarios.

Index Terms—RFID, approach detection

1 Introduction

Passive Radio Frequency Identification (RFID) tags have been increasingly deployed in many applications [1], [2], such as logistics, retailing, etc. Thanks to the capability of automatic identification and wireless energy harvesting, RFID tag is utilized to localize or track properties. Recently, there is growing interest in human motion detection using backscattered RFID tags. Human motion is an appearing mean of interaction with computing devices. In particular, hand movement can reflect what we are doing or what we intend to do next. Detecting hand approach and departure behaviors is already an essential function for a wide spectrum of applications. We identify the following user cases for approach detection.

- In a supermarket or shopping mall, objects are attached with passive tags. Customizers can approach an item to obtain its price, production site, and other information.
- A number of items are placed in house. For infant/elder care, approach detection can create alarms when a hand is approaching towards dangerous or fragile objects.
- Hand approach detection can be utilized in smart home environment, such as approaching to a tag attached on the coach to activate a remote switch, turn on the light, or turn down the music, etc.

Current approach detection schemes mainly rely on technologies that use imagers, biological signals (such as electromyography (EMG), electroencephalography (EEG)), or dedicated sensors (for example, tactile sensors). However, existing solutions are either impractical or extremely expensive. The imager based approach uses cameras to capture a sequence of images or videos containing the user's movements or appearance and then utilizes pattern recognition techniques to identify the human movements [3], [4]. A critical limitation of imager based approaches is that cameras usually demand good lighting conditions or image quality. Moreover, privacy concern also raise barrier for their implementation. Device-based solutions, such as those using the Brain and Machine Interference (BMI) technology [5], [6], are inconvenient and inflexible for users' daily life. Another recent advance is to embed specific sensors, including magnet sensors, micro-switches, and tactile sensors etc., in physical space to monitor the human gestures or movements [7], [8]. These approaches suffer from high deployment cost. In a short summary, above solutions all require dedicated devices/infrastructures, leading constraints to users or incurring high overhead.

In this paper, we propose a device-free approaching detection system based on backscatter communication of

- *H. Ding is with the School of Electronic and Information Engineering, Xi'an Jiaotong University, Xi'an, Shaanxi 710049, China, and the State Key Laboratory for Novel Software Technology, Nanjing University, Nanjing 210008, P.R. China. E-mail: dinghan@xjtu.edu.cn.*
- *C. Qian is with the Department of Computer Engineering, University of California at Santa Cruz, Santa Cruz, CA 95064. E-mail: cqian12@ucsc.edu.*
- *J. Han is with the Institute of Cyberspace Research, College of Computer Science and Technology, Zhejiang University, China. E-mail: hanjinsong@zju.edu.cn.*
- *J. Xiao is with the Department of Electronic Science and Technology, ChangAn University, Xi'an, Shaanxi 710064, China. E-mail: xiaojian@chd.edu.cn.*
- *X. Zhang, G. Wang, W. Xi, and J. Zhao are with Department of Computer Science and Engineering, Xi'an Jiaotong University, China. E-mail: {xjzhang, xiwei, zjz}@mail.xjtu.edu.cn, wangge@stu.xjtu.edu.cn.*

Manuscript received 1 Jan. 2018; revised 3 July 2018; accepted 17 Sept. 2018. Date of publication 28 Sept. 2018; date of current version 28 Aug. 2019. (Corresponding author: Xingjun Zhang.)
For information on obtaining reprints of this article, please send e-mail to: reprints@ieee.org, and reference the Digital Object Identifier below.
Digital Object Identifier no. 10.1109/TMC.2018.2872558

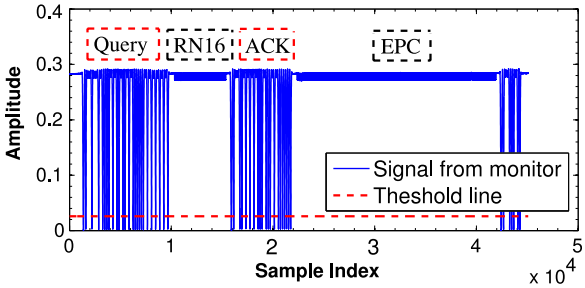

Fig. 1. EPCglobal C1G2 backscatter protocol. Signals from both endpoints are collected in our experiment.

Ultra High Frequency (UHF) passive Radio Frequency Identification (RFID) tags, called APID. APID has no constraints to users and can reuse the existing RFID infrastructure, which is widely deployed in many daily life applications [9]. The basic idea is motivated from the following observation of our preliminary experiments. The approach or departure of a hand towards a tag will cause evident and special variations of its backscatter signals. To collect these signals, we introduce a monitor to APID. In practice, we deploy the monitor over Universal Software Radio Peripheral (USRP) [10] for passively overhearing the communication between the reader and tags. Thus, by analyzing and estimating the signal variations, APID can detect the approach and departure behaviors towards tags.

We formally model the tag's signal changes when an individual's hand approaches or departs from it. Then APID calculates the power spectral density (PSD) of every tag's signal, and determines the behavior from the trends of PSD. There is a critical challenge in APID when there are multiple tags coexisting. The monitor needs to correlate the collected signals to their source tags, given that there is no effective statistical features that can differentiate tag when a human body moves around. To solve this issue, we design a decoder algorithm to accurately separate different tags' data. Then we extract Coefficient of Variation (CV) feature of continuous tag signals to determine the approach target of the user.

We have implemented a prototype of APID using a commercial Impinj RFID reader model R420 and passive tags from two manufactures (i.e., Impinj and Alien). The monitor is implemented by USRP N210 with a SBX daughterboard. Our system follows *the extensible RFID model* [1], [11], where the RFID reader used for APID can be reused for other applications such as ordinary tracking and identification of items. The monitor in our system only passively listens on the communication between the reader and tags, analyzes the tag signal variation and reports the approach and departure behaviors to enable extra functions. Thus, our system can be easily deployed with existing RFID system and reduces hardware cost. In particular, APID operates in the area covered by its monitor's antenna. For example, if we deploy the antenna under a table such that the surface of the table is effectively under surveillance, APID can conduct hand-approach detection to the tagged objects on the whole table.

We conducted extensive experiments in various scenarios. Fifteen volunteers participate in the experiments. The experimental results show that APID can achieve high estimation accuracy. For example, APID correctly detects the approach and departure behaviors with the accuracy of about 93 percent; and in nearly 88 percent of our tests, APID can identify the real target of a volunteer with up to ten tags coexisting.

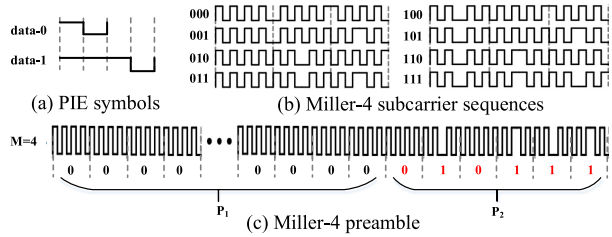

Fig. 2. RFID modulation and data encoding schemes.

2 Background and Overview

In this section, we introduce the backscatter communication protocol of UHF passive RFID systems. We then take an overview of APID.

2.1 Backscatter Communication in RFID Systems

Communication in passive RFID systems is based on backscatter radio links. Passive tags carry no battery or radio transmitter. Instead, they harvest power from the reader. The EPCglobal Class-1 Generation-2 (i.e., ISO 18000-6C) protocol is the mainstream industrial standard detailing the interaction between a UHF RFID reader and passive tags. EPCglobal C1G2 is a reader-talks-first protocol [12]. The reader chooses the communication parameters and controls the process based on a slotted ALOHA mechanism. Generally, the communication starts with a reader's `QUERY` command. Each tag randomly selects a slot to reply with a 16-bit random number, i.e., the `RN16`. If the reader receives only one tag response and can decode the number, it sends an `ACK` to acknowledge the tag. Then the tag replies with its Electronic Product Code (`EPC`), e.g., ID. Fig. 1 shows the signals from both endpoints during the procedure captured by our USRP monitor, which clearly illustrates the standard communication process.

2.2 Modulation and Data Encoding

In this section, we briefly introduce the modulation and data encoding methods of EPCglobal C1G2.

2.2.1 Reader-to-Tag Communication

Due to the limited computing capability of passive tags, an RFID reader uses Amplitude-Shfit Keying (ASK) modulation. In ASK, digital bits are represented as variations in the amplitude of a carrier wave. The reader uses Pulse Interval Encoding (PIE) to encode data. As shown in Fig. 2a, a high value and a same-length low value combine to represent a bit '0'. The combination of a longer high value and a short low value represents a bit '1'. In addition, high values correspond to transmitted continuous wave (CW), whereas low values represent attenuated CW. Since the reader supplies energy for passive tags through these high values, PIE encoding is suitable for tag's power-harvesting property. The design of proposed tag EPC extraction algorithm (Section 4.1) is based on this characteristic of PIE.

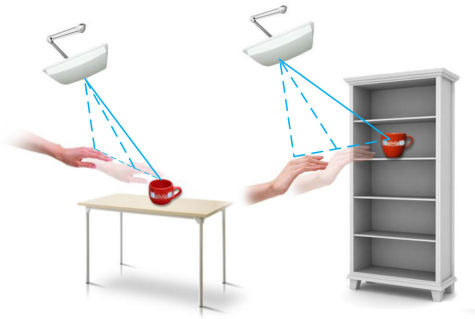

Fig. 3. The model of RF signal transmission with approaching behaviors. The monitor is hidden under the table or behind the shelf.

2.2.2 Tag-to-Reader Communication

The encoding scheme for the tag-to-reader link is determined by the reader. Optional schemes include FM0 (i.e., bi-phase space) and Miller-modulated subcarriers (Miller-2, Miller-4, Miller-8). The Miller schemes are binary-phase-shift-keyed. It provides better interference rejection than FM0. A higher-value Miller method corresponds to slower data transmission. In our system, we config the coding scheme as Miller-4 for a good balance. Miller-4 means that four cycles of the subcarrier are needed for encoding each bit. As shown in Fig. 2b, a bit '1' of Miller-4 contains a state transition in the middle of its four symbols, while a bit '0' does not, which is the basis of our proposed EPC decoder algorithm (Section 5.2).

2.3 System Overview

APID consists of three main components, a commercial RFID reader (Impinj Reader R420), a number of objects (each of them attached with a tag), and a monitor (USRP N210 with a SBX daughterboard). The reader queries tags by transmitting commands and CWs. The role of the monitor is to passively listen the communication between the commercial off-the-shelf reader and tags, analyzing the backscattered signals from tags, and differentiating the human hand behaviors.

APID works in two scenarios. *1) Single-object scenario.* When a human hand is approaching or departing from an object, APID should detect this movement. *2) Multi-object scenario.* When the human hand is approaching an object among multiple objects, APID is able to recognize which object s/he is approaching.

3 Model and Insight

In this section, we build a theoretical model to analyze the impact of human approach behaviors to backscatter signals.

Due to the multipath effect, in real environments the RF wave emitted from a reader to query a tag usually interacts with many other objects around the tag. Hence the integrated waves consist of the ones along direct path between the reader and tag, and those that are *reflected*. For backscatter communication, the most important and ubiquitous reflectors are the floors and walls. Since the ambient factors are stable, we can conclude that the integrated signal will remain nearly time invariant with no human interference. On the other hand, when there is a human hand moving towards the tag, another reflected wave will be introduced. In this case, we can describe the newly integrated signal by the following equation:

$$S^{'}\cos\left(wt\right) = \underbrace{s_c\cos\left(wt+\theta_c\right)}_{constant} + \underbrace{s_h\cos\left(wt+\theta_h\right)}_{variation}, \quad (1)$$

where s_h denotes the signal induced by the hand. As indicated by Eq. (1), the new signal is composed of two parts, i.e., the constant part and the variation part. It indicates that the reflected signal caused by the hand is of counter-intuitively importance. When the hand is moving, the traveling path of RF signals between the constant part and the hand-reflected part changes. In theory, a change of 8 cm (a quarter of the wavelength) along that path produces a 90° phase shift, resulting in a change of the signal from a maximum value (or minimum value) to zero. This means that continuous integrated signals will repeatedly oscillate as the hand is approaching the tag or moving away from it.

We further consider the amplitude of the oscillation. As illustrated in Fig. 3, the reader antenna is mounted on the ceiling, illuminating tags within its reading region. A hand is getting closer to a tagged cup. We know that during this procedure, the reflection signal distance (i.e., reader-hand-tag distance) is getting shorter. It is known that a shorter path incurs lower attenuation to the signal, resulting in larger amplitude. Thus, we can infer that when the hand is getting closer to the tag, the amplitude of the oscillation will become larger. Conversely, the amplitude will decrease when the hand is moving away from the tag. Thus, we have the following insight about RF signals corresponding to the hand movement. *The continuous RF signals oscillate with the hand movement and can be utilized to differentiate approach from departure based on the variation tendency.*

4 Identifying Approach and Departure Behaviors

In this section, we present the method to analyze backscatter signal variations in practical RFID systems and validate the theoretical results.

4.1 Signal Preprocessing

In UHF passive RFID systems, a commercial reader can query a tag and receive its replies for hundreds of times per second. The monitor device can record the signals of each complete inventory on a specific tag, as shown in Fig. 1. To verify the aforementioned theoretical analysis and further identify gestures, we need to extract the backscatter signals from the collected mixed signals.

In a common backscatter communication process, two types of messages are sent by a tag, i.e., RN16 and EPC. We choose to use EPC as the source signal for subsequent analysis. EPC is the unique identifier of a tag, consisting the ID information. We develop the `EPC Filter` module in the monitor, which can accurately retrieve the EPC message from communication signals. The EPC filter has two procedures: coarse-grained segmentation and fine-grained localization.

4.1.1 Coarse-Grained Segmentation

Coarse-grained segmentation module aims to differentiate between reader commands and tag replies. After this

TABLE 1
Reader Commands and Parameters

Command	Descriptor	Bit
Query	1,000	22
QueryRep	00	4
QueryAdjust	1,001	9
ACK	01	18

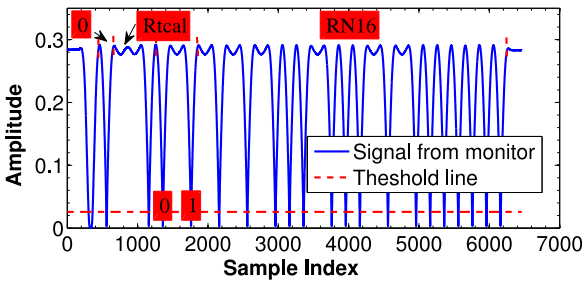

Fig. 4. ACK command under PIE encoding collected by the monitor.

TABLE 2
Reader Command Components and Parameters

Command	Time duration	Length	Range
RTcal	[2.5Tari, 3.5Tari]	600	480∼720
TRcal	[1.1RTcal, 3.0RTcal]	700	560∼864
Data-0	1 Trai	220	176∼264
Data-1	[1.5Tari, 2.0Tari]	360	288∼432

module, we can derive the coarse EPC sequence. The strategy is detailed in the following.

According to the EPCglobal C1G2 protocol, tag replies EPC after receiving an ACK command from the reader. Based on this fact, we can derive the coarse-grained EPC segment between the ACK and a subsequent reader command. The reason why we utilize reader commands to seek for EPC is: the reader's signal has higher SNR and larger amplitude, which makes it easier to be located and decoded. Table 1 lists the reader's commands and their parameters specified by the protocol. We can see that every command has its unique descriptor. It inspires us to locate an ACK easily by decoding its descriptor. As Fig. 4 shows, starting with a frame-sync (composed of a fixed-length start delimiter, a data-0, and an R⇒T calibration (RTcal)), ACK has two parts: a 2-bit descriptor ('01') and a 16-bit RN16. We choose a low threshold (Fig. 1) to locate reader commands and then decode the command by comparing every pulse width with Table 2. These parameters are the basic components of every reader command, and the lengths of them are specified by the protocol, among which *Tari* is in the range of 6.25 μs to 25 μs, and the choice of Tari shall in accordance with local radio regulations (Tari = 25 μs in our implementation). For better fault-tolerance, we extends the length by $\pm 20\%$.

4.1.2 Fine-Grained Localization

After coarse-grained segmentation module, we get the EPC segment between the end of ACK and the begin of the next command; nevertheless, this EPC segment includes many carrier samples, such as the first 500 samples shown in Fig. 5a. Falsely including these samples may affect the

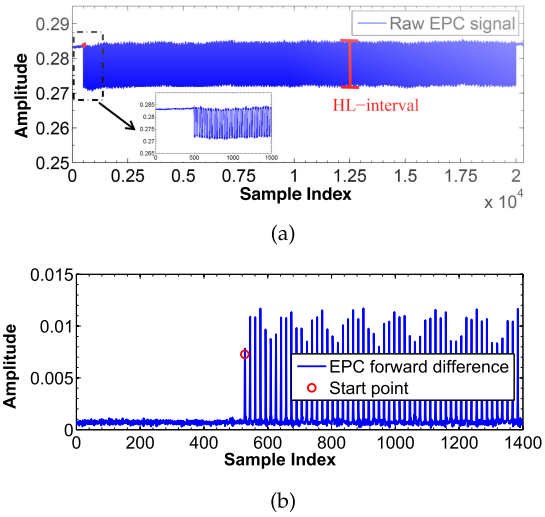

Fig. 5. Fine-grained EPC localization. (a) The raw EPC segment. (b) The AFD of the raw EPC samples.

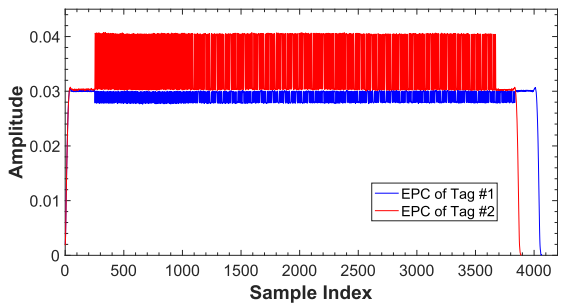

Fig. 6. Tags' EPC signals locate in different positions compared to the carrier.

subsequent signal energy estimation. Therefore, we need to further find the start point of the EPC segment from the raw signal samples. We term this process as fine-grained EPC localization.

In our experiments, we observe that the signals of different tags may locate in different positions. As shown in Fig. 6, sometimes a tag signal (Tag #1) is higher than the carrier but in some other cases it is lower than the carrier (Tag #2). As a result, we cannot determine a certain threshold to find the start point. To solve this problem, we apply the *Absolute Forward Difference* (AFD) method to accurately localize the start point of EPC.

Given an EPC sequence $E = (e_1, e_2, \ldots, e_K)$, the AFD value is calculated by

$$\triangle E = |e_{k+1} - e_k|, k = 1, 2, \ldots, K-1. \quad (2)$$

The AFD result of the EPC signal in Fig. 5a is shown in Fig. 5b. Utilizing the obvious amplitude difference of carrier signals and real EPC signals, we can now employ a simple threshold method to quickly find the first sample of E, as the red circle outlined in two subfigures.

4.2 Identifying Behaviors

After signal preprocessing, the system obtains the tag EPC sequences. In this section, we verify the theoretical model aforementioned and utilize the EPC power variation trend to identify approach and departure behaviors.

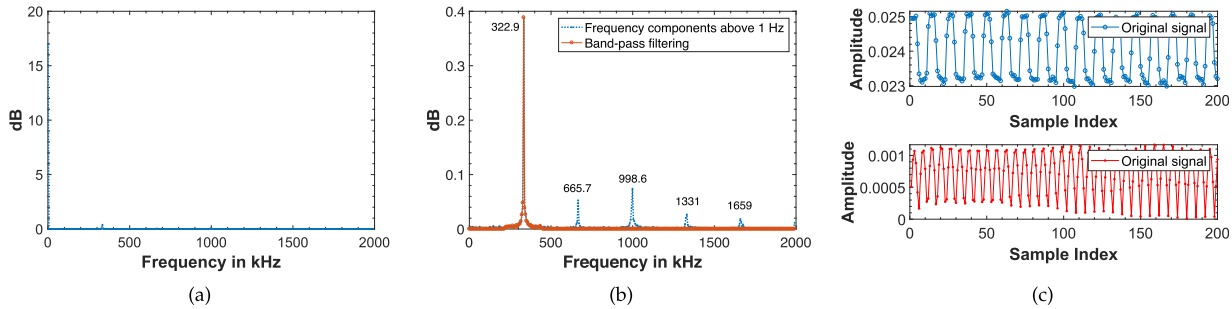

(a) (b) (c)

Fig. 7. (a) Magnitude response of one tag EPC. (b) Frequency components above 450 kHz or below 216 kHz have been zeroes. (c) Original and recovered EPC signal.

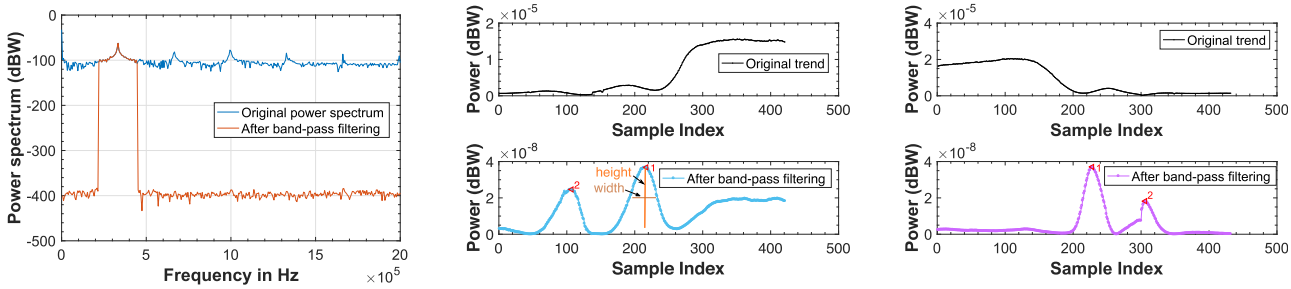

(a) (b) (c)

Fig. 8. (a) Power spectrum of one tag EPC. (b) Power variation of approaching behavior. (c) Power variation of departure behavior.

4.2.1 Frequency-Domain Analysis

Before measuring the power trend, we first conduct the frequency-domain analysis. The frequency-domain representation of the EPC could tell the signal's magnitude at each frequency and help to optimize the signal quality.

The data independence should be guaranteed when conducting the analysis. To this end, we adopt the P_1 part (Fig. 2) of the EPC preamble as the source signal (since the waveform of P_1 is constant for various tags). Note that in the following the EPC is referred to P_1.

We use Fast Fourier Transform (FFT) to observe the frequency content of a tag's EPC signals. As shown in Fig. 7a, the magnitude at 0 Hz is around 17 dB (much higher than those at other frequencies), which is the DC component, corresponding to the mean amplitude of the original EPC data. Since the variation trend of sequential tag signals is our main concern, we can safely ignore the DC component and focus on the other frequencies. Fig. 7b illustrates the magnitude responses above 1 Hz. As shown in the figure, the signal has fifth order distortion. The main frequency (F_m) is concentrated at around 333 kHz. Generally, harmonics are as a result of either unbalanced or non-linear loads, which are undesirable in power systems since they will cause the distortion of useful signal. The power of harmonics will lead to the variation of the envelope of time-domain signal. To weaken the effects of harmonics, we only keep the frequency components around F_m (i.e., [F_m - α, F_m + α], α = 150 Hz in the implementation). We remove the frequency components out of above range (making the magnitudes equal to zero) directly from the FFT output, which actually acts as bandpass filtering. To check the effect, we project the filtered signal back to time domain using Inverse Fast Fourier Transform (IFFT). As Fig. 7c shows, the mean amplitude of the recovered signal is reduced, but its main shape is almost unchanged.

4.2.2 Behavior Identification

In this part we track the power variation of sequential EPCs for identifying approach and departure behaviors. First, we utilize Power Spectral Density (PSD) to measure the power of an EPC signal. PSD is an average power estimation over a frequency interval at which a point is defined (the resolution bandwidth). Fig. 8 illustrates the power spectral of the original EPC and the filtered EPC. We can observe five peaks at F_m and harmonics for original EPC. The plot tells that harmonics play important roles in power spectral. Hence taking all harmonics into consideration might drown the information carried by the main frequency components. To validate above conjecture, we conduct a group of proof-of-concept experiments. We invite a volunteer to move his hand approaching to a tagged cup, then move away. The monitor records the communication signals during this procedure. Note that we take the mean value of an EPC power spectrum (Fig. 8a) as the representation of an EPC power. Figs. 8b and 8c show PSD variations of approach and departure behaviors, respectively. We observe that there are two peaks, representing that the volunteer moves his hand with a length of about 30 cm (Since the wavelength is about 32 cm, which means a movement of about 16 cm will lead to an oscillation). The results also validate our insight gained from the theoretical model. Human hand movements incur energy oscillations to the replies (e.g., EPCs) of tags, and the movement direction (approach or departure) can be deduced from the vibration increase or decrease. In addition, the bandpass filter helps to make the phenomenon more noticeable.

Specifically, to distinguish two opposite gestures, we utilize the peak detection algorithm. As shown in Fig. 8b, two parameters, *height* h and *width* w (empirically determined) are defined to remove the local maxima. We detect the peaks and sort them in a descending order. Then the approaching and departure behaviors can be distinguished

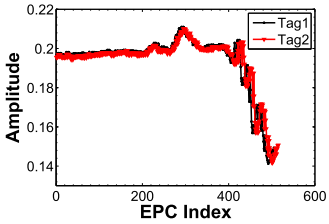

Fig. 9. Amplitude changes of two tags when a hand is approaching one of them.

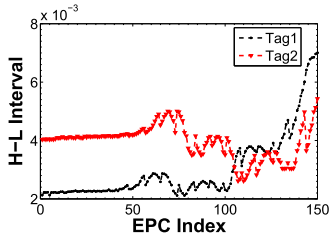

Fig. 10. H-L interval changes of two tags when a hand is approaching one of them.

directly from the sequentially sorted labels. For example, Fig. 8b illustrates the approach behavior, and its sorting label is '21'. On the other hand, the sorting label of departure behavior shown in Fig. 8c is '12'. Note that the motion segmentation, i.e., the start point detection of the motion, can be conducted using KL divergence metric [13]. Since when there is no motion towards a tag, the signal of the tag will be relatively stable. However, when a motion happens, the signal will vibrate rapidly. In addition, ambient noise, such as the variation introduced by someone walking around, can be easily filtered by the preprocessing (e.g., comparing the DTW distance with a predefined threshold), since the signal variation tendency is irregular and inconsistent with either the approach or departure behavior.

5 Multi-Object Scenarios

In the previous section, we solve the problem of identifying whether a user is approaching an object in a single-object scenario. However, in real circumstances, like a table or a shelf, there could be more than one object, each of which carries a passive tag. In this section, we present the solution to find the true approach target of the human hand in multi-object scenarios.

5.1 Challenges

According to the specifications in EPCglobal C1G2, multiple tags reply their EPCs to the reader in random orders in one inventory round using the slotted ALOHA protocol. Therefore, APID needs to resolve two main problems. First, it should differentiate tag signals based on their sources. Second, it should find the tag whose signal has the most prominent change, which indicates the target of an approach behavior.

To begin with, we attempt to pursue proper features in the signal level to solve the first problem. We put two tags on a table with 30 cm in between. Then a volunteer moves his hand to one of them. We try mainstream features used by prior works in fingerprinting wireless signals, including Entropy, Energy Spectrum Density (ESD), Pulse Amplitude, Mean Square Error (MSE), Mean, and Variance, etc. Unfortunately, during the movement of user's hand, the tag signal varies with time, and we could not find appropriate features which can uniquely and stably represent a specific tag. We present the attempt of using two representative features as following.

Amplitude. Fig. 9 plots the amplitude of these two tags' EPC signals. We see that they almost overlap with each other. The reason behind may be that tags' signals are all modulated based on the reader transmitted carrier waves, so all tag signals shall change consistently as the carrier.

HL-interval. In addition, due to the hardware heterogeneity [14], when modulating a same logic data '0' or '1', tags yield different intervals between the high level and low level values. We denote such an interval as a HL-interval. We plot an example of HL-interval in Fig. 5a. As shown in Fig. 10, the HL-interval of a tag is distinct and stable for the first 50 points. It seems that HL-interval is a good choice for differentiating tags. What disappoints us is that when the hand is moving (starting from the time of near 50th point), both tags' signals are influenced. Their HL-interval values cross with each other at about 110th point and become indistinguishable.

In summary, an approach behavior has complex impact on the tag signal, and it is difficult to find a unique feature to distinguish signals from different tags.

5.2 Differentiating Tag Signals

In this section we solve the first problem: differentiating signals from different tags. The monitor can capture EPC messages but it cannot distinguish them, i.e., extracting the IDs of these tags like a COTS reader. Thus, leveraging the architecture of EPC memory and characteristics of Miller-4 encoding (refer to Section 2.2.2), we implement an `EPC decoder` module, which includes a `recoder` algorithm and a `decoder` algorithm.

It is worth to briefly introduce the composition of the EPC memory. As the ID or identifier of each tag, the EPC memory contains PC, EPC and CRC-16, which are stored in the order of the most significant bit first (MSB). In particular, PC is 16-bit long, and its first 5 bits (denoted as $\mathtt{PC}_5$) define the EPC length. For example, PC_5 = 00110 means the EPC is 6-word long. In addition, the maximum length of EPC is 8 words (e.g., 128 bits) specified by EPCglobal C1G2. For simplicity, we use a part of the EPC signal collected from a 96-bit long tag to illustrate the following algorithms.

5.2.1 Recoder

For passive RFID systems when tag EPC is encoded in Miller-4, it means that a bit contains 4 subcarrier cycles, as illustrated in Fig. 2. With the monitor sampling rate of 10M/s, the number of samples of a subcarrier cycle (representing symbol '0', as shown in the upper small figures in Fig. 11) is constant, i.e., about 30 in total, while 15 are for high level values, other 15 are for low levels. We recode such a subcarrier cycle (with same length of high level and low level) as symbol '0'. Our recoder detects the last point of the low state for every subcarrier, as the red points shown in Fig. 11. Hence, the recoded symbols '0' and '1' can be differentiated by comparing the interval (ΔI) of adjacent red

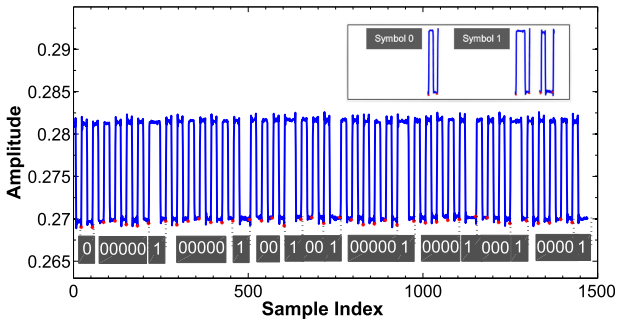

Fig. 11. An example of the recoder.

points. If $\Delta I > M$, we get a symbol '1' ($M = 40$ in our implementation). Otherwise, we get a symbol '0'. Fig. 11 illustrates a part of Miller-4 encoded EPC, composed by P_2 of preamble (e.g., 010111, refer to Fig. 2c) and PC_5 (e.g., 00110). The recoded sequence is marked in grey boxes, which is the input of the following decoder algorithm.

Algorithm 1. EPC Decoder

Input: Symbol sequence: $S = (s_1, s_2, \ldots s_n)$
Initial $b : K$
The number of bits need to be decoded: L
Output: Bit sequence: $B = (b_1, b_2, \ldots, b_L)$

$i \leftarrow 0, b \leftarrow K, e \leftarrow K + 3$
while $i < L$ **do**
  $t \leftarrow S(b : e)$
  if $t(2) == 1$ **then**
    $B(i) = 1, b \leftarrow e + 1, e \leftarrow b + 3$
  else if $t(3) == 1$ **then**
    $B(i) = 1, b \leftarrow e, e \leftarrow b + 3$
  else
    $B(i) = 0$
    if $t(1) == 1$ **then**
      $b \leftarrow e + 1, e \leftarrow b + 3$
    else
      $b \leftarrow e, e \leftarrow b + 3$
    end if
  end if
  $i \leftarrow i + 1$
end while

5.2.2 Decoder

The decoder algorithm is designed by leveraging the characteristics of Miller-4 encoding. That is, every four subcarrier cycles construct one bit, and bit 1 has an state transition in the middle. We translate every continuous 4 symbols into one bit, and determine the value of the bit by checking the position of the symbol '1'. If symbol '1' locates in the middle of 4 symbols (the 2nd or 3st position), we translate such 4 symbols as a bit 1. Otherwise, we get a bit 0. Moreover, the begin index and end index of the current 4 symbols are determined by the former 4 symbols. The detail of the decoder algorithm is elaborated in Algorithm 1, in which b and e denote the begin index and end index respectively.

As an example, we execute the algorithm on the symbol sequence in Fig. 11. In this example, the input $S =$ '0000001000001001001000001000001000100001', $L = 11$, $K = 1$. The dotted boxes in Fig. 12 illustrate the procedure of our

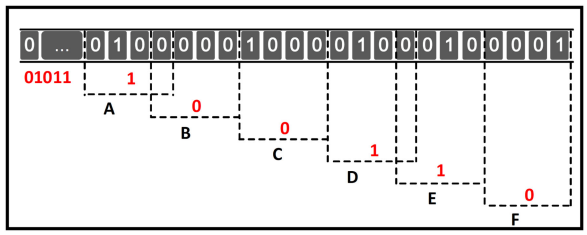

Fig. 12. Illustration of the EPC decoder algorithm.

algorithm. For example, we get a bit 1 from the 4 symbols '0100' in box A. Based on the position of symbol '1' (i.e., 3st position), we get the translated bit 0 and the next 4 symbols '0000', as shown in box B. Ultimately, the output bit sequence $B = 01011100110$, implying that $P_2 = 010111$ and $PC_5 = 00110$. This well matches the corresponding part in the real EPC. The result proves that our decoder is able to distinguish different EPCs effectively. Note that above methods can be easily extended to other encode/decode mechanisms adopted by existing COTS passive RFID systems, such as Miller-2 and Miller-8, etc.

5.3 Identifying the Approach Target

Using the unique EPC code, we can separate signals of different tags. We then aim at figuring out the true target of the approach behavior among multiple objects. In APID, our objective is to extract a feature from the replied EPC signals, which can well profile the most prominent influence corresponding to a human hand movement.

In real circumstances, tags are different in their H-L intervals. We observe that the signal variation of a tag with high H-L interval is almost always more obvious than that of a tag with low H-L interval. We tested 10 pairs of tags that 8 of them behave like this. This may cause false alarms when identifying the real target if the user is approaching to the tag with low H-L interval. We conduct a proof-of-concept experiment to show this phenomena. We put two tagged objects on the table (among which Tag1 has higher HL-interval), and ask the volunteer to move his/her hand to them, one at a time. The power trends of two tags are showns in Figs. 13a and 13b. From the results we see that no matter the volunteer approaches to Tag1 or Tag2, Tag1 (with higher HL-interval) always has larger power variation.

To address above problem, we propose to utilize the metric of *coefficient of variation*. To guarantee the data independence, we calculate the *coefficient of variation* of P_1 (a part of the EPC preamble) to reflect the influence. CV is a standardized measure on the dispersion of a probability distribution, defined as

$$CV = \sigma/\mu, \tag{3}$$

where σ is the standard deviation and μ is the mean. It shows the extent of variability in relation to the mean. CV is a dimensionless number, and the actual value of CV is independent of the unit of the measurement. Hence it is suitable for comparison among the data with different means and H-L intervals. In APID, we can treat the samples of P_1 as a random source, and calculate CV for every P_1 of continuous tag signals. To evaluate the effectiveness of CV, Figs. 13c and 13d show the results of the same experiment. When the hand approaches Tag1, its CV is larger than that of Tag2.

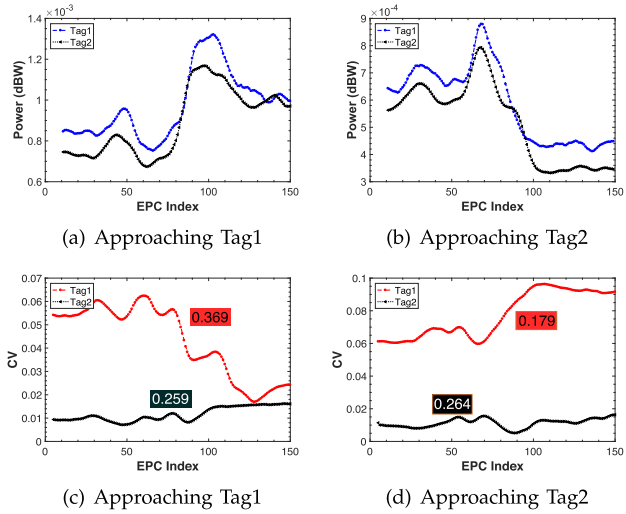

(a) Approaching Tag1 (b) Approaching Tag2

(c) Approaching Tag1 (d) Approaching Tag2

Fig. 13. PSD and CV variations of EPC sequences.

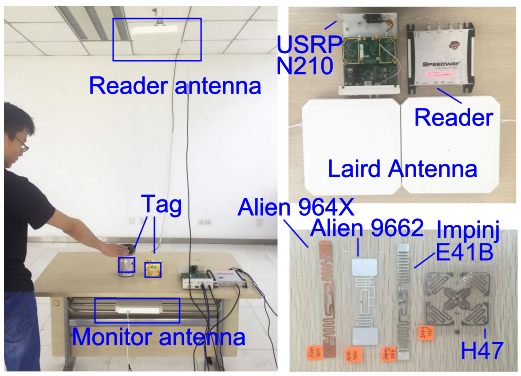

Fig. 14. System prototype.

On the contrary, when the hand approaches Tag2, the CV is opposite. Thus, we propose to regard the tag which has the maximum CV variation as the target that the user actually moves his/her hand to.

6 Implementation and Evaluation

In this section, we present the implementation and evaluation of APID.

6.1 Experimental Setup

We build APID using a COTS Impinj Reader R420, 20 passive tags of four tag models from two manufacturers (i.e., Alien 9640, Alien 9,662, Impinj E41B, and Impinj H47, each of them costs 5-10 cents). We use a USRP N210 with a SBX daughter board as the monitor [10] to record the physical layer signals transmitting between the reader and tags. The antennas (model Laird A9028R30NF) used by the reader and monitor are both directional. The size of antenna is 25.4 cm × 25.4 cm × 3.8 cm and with 8 dBi gain.

The reader antenna is mounted on the ceiling, about 3m apart to the tags. We attach tags to various objects, such as bottles, books, cartons, etc., to verify the effectiveness of APID. Tagged objects are placed following two common display modes, horizontal mode (i.e., simulating a table) and vertical mode (i.e., simulating a shelf). The monitor antenna is deployed under the table or on the back of the shelf. The

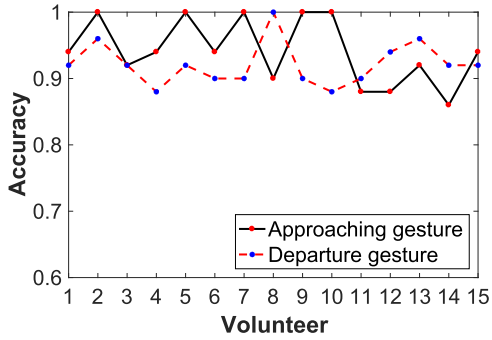

Fig. 15. Overall accuracy versus human diversity.

principle of positioning the monitor is to make sure that the monitor can receive the RF signals backscattered from the tags, while the line-of-sight transmissions between the monitor's antenna and tags are not always blocked. In addition, when conducting the approaching behaviors, the user stands besides the table/shelf and moves his/her hand towards the object with the length of a armspan.

6.2 Accuracy of Single Tag Scenario

We evaluate APID's accuracy of recognizing approach and departure gestures under different conditions.

6.2.1 Overall Performance

We first investigate the overall performance of approach and departure detection. The experimental scenario is the same as Fig. 14. One tag is placed on the table simulating the tagged object. We invite fifteen volunteers to conduct this series of experiments. Their heights vary from 160 cm to 180 cm. A volunteer first moves his/her hand approaching to the tag, then departing from it, by repeating 50 times. During these experiments, the position of each volunteer is specified ahead, but their approaching motions are performed arbitrarily. The results are shown in Fig. 15. The average accuracy for the fifteen volunteers maintains in a high level: 93.1 percent. Specifically, the minimum accuracy can still reach 88 percent for volunteer 4's departure behaviors. This indicates that APID can effectively identify the approach and departure behavior, and it works well across different users.

6.2.2 Distance between the Hand and the Tag

We then study the effect of distances between the hand and the tag on the detection accuracy. Note that the distance here represents the nearest distance during the hand movement, and the volunteer moves one arm long. Fifteen volunteers participate in this experiment. Each volunteer performs the approach and departure behaviors for 30 times in each distance, without blocking the tag. We identify the behavior through the trend of continuous EPC power values. The results are shown in Fig. 16. The bar in this figure shows the probability that the power trend follows our deduction, i.e., APID correctly determines the gesture. The results show that when the distance increases, the detection accuracy decreases gradually. The mean detection accuracy remains high ($>90\%$) when the distance is smaller than 30 cm. It means that the data collected when the hand is 30 cm away from the object is enough for APID to differentiate the gestures. However, when the distance enlarges to 60 cm,

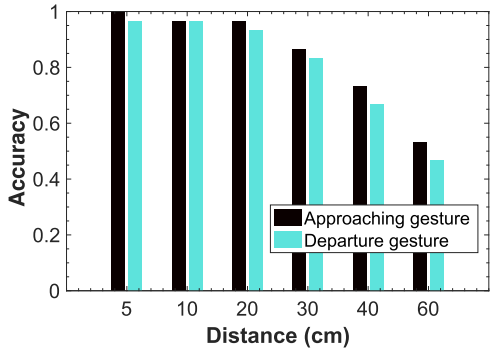

Fig. 16. Accuracy versus hand-to-tag distances.

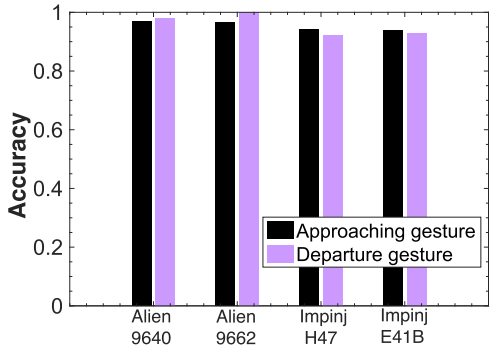

Fig. 18. Accuracy versus tag diversity.

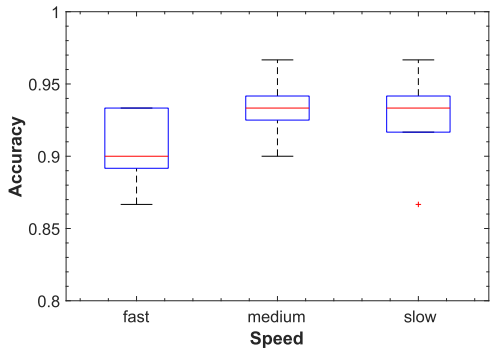

Fig. 17. Accuracy versus approaching speeds.

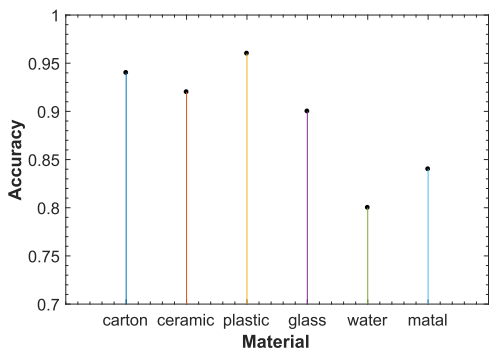

Fig. 19. Impact of materials.

more than half of the gestures become unidentifiable. The reason is that when the hand moves farther away from the tag, the influence of the hand reflection to tag signals becomes smaller, resulting in more unapparent oscillations. Our system provides a solution for hand approaching detection for arm-reachable applications. In common cases, we think 30 cm is reasonable for arm-reachable scenarios.

6.2.3 Approaching Speed

The movement speed is an essential factor when performing the approach behavior. Generally, different users would move their hands at various speeds. With this observation in our mind, we test the impact of approaching speed to our detection algorithm. We ask the volunteers to conduct the approach behaviors, and separate their speeds into three categories (e.g., fast, medium, slow). Specifically, the time duration of each category is about 1.5 s, 3.5 s, and 5.6 s, respectively. For each category, we have 5 groups of experiments, and each group has 20 times of approach behaviors. Fig. 17 shows the average accuracy under each speed. The results show that the hand moving speed has little impact to the detection accuracy, i.e., the average accuracy still retains above 90 percent. The reason is that a commodity UHF reader, e.g., Impinj R420, is capable to read more than 300+ tags per second. Such a high rate allows the reader to collect a large number of responses from the tag. The sufficient samples extracted from those responses would guarantee a fine-grained monitoring on the hand approach movement, even if the movement speed is very high.

6.2.4 Tag Diversity

Then we evaluate if APID is compatible with different tags. We use four kinds of passive tags from two manufacturers (Alien 9640, 9662; Impinj H47 and E41B) in this group of experiments. During each experiment, a volunteer was asked to move his/her hand towards a specific tag, or away from it. The result is shown in Fig. 18. We find the detection accuracy of Alien tags is a little higher than that of Impinj tags, which exceeds 96 percent for both approach and departure behaviors. We conjecture the reason may lie in the antenna designs. Different tag models have different antenna and IC designs, which influence the tag backscattered signals (as well as the detection performance). Generally, the result also indicates that our approach detection algorithm is applicable for different kinds of tags.

6.2.5 Materials

Current UHF RFID systems are designed to operate around the frequency of 900 MHz, with which the tags function well on the surface of most common materials, including glass, paper, etc. However, RF transmission can be significantly affected by certain materials, such as metal and water, either completely reflecting an incident wave or absorbing it. To test the essential effect, we attach an Alien 9640 tag on certain objects that are composed with different materials. Fig. 19 shows the approach detection accuracy. The results show that the accuracy of APID does relate to the type of material. It is worth noting that if we put the tag directly on the metal, it becomes invisible, i.e., no replies are received by the reader. However, if we only let half of the tag antenna on the metal, the detection accuracy can still reach about 85 percent. In addition, APID experiences worst performance when we put the tag on a mineral water bottle. We find that the tag power is lowest in this case, hence the power variation is hard to profile. In a nutshell, for those applications where tags need to be attached near metal or

TABLE 3
Performance over Different USRP Sampling Rates

USRP sampling rate	2 M/s	4 M/s	10 M/s
Accuracy	0.86	0.92	0.94
Storage overhead per motion	0.6 M	1.2 M	2.7 M

water, we recommend dedicated tags, such as anti-metal and anti-water UHF tags.

6.2.6 Sampling Rate

We further examine the impact of the USRP's sampling rate to the stability of proposed method and detection accuracy. In our implementation, the default sampling rate is 10 M/s. We change it to 2 M/s and 4 M/s, and test the system performance. We ask five volunteers to conduct 100 experiments under each sampling rate, respectively. Table 3 demonstrates the performance of approach detection. We find that the accuracy under 4 M/s or 10 M/s is higher. If using the 2 M/s setting, the accuracy is relatively low. In practice, the sampling rate determines the number of points APID can collect within a pulse. In general, more points enable a more fine-grained representation of the signal. Thus, the highest accuracy can be achieved if using the 10 M/s sampling rate. On the other hand, high sampling rate would increase the storage overhead. Table 3 also lists the average EPC data storage of one approach motion (including 200 EPCs). Considering the long-term running of the system, we recommend to use the 4 M/s sampling rate for balancing the storage overhead and accuracy.

6.2.7 The Number of Tags

To test the system performance when different number of tags coexisting in the system, we conduct a group of experiments. For each number, we check how APID can recognize the approach behavior. The results are shown in the new figure, Fig. 20. We can see that when the number of tags are smaller than 10, the detection accuracy can reach above 90 percent. When continuously enlarging the number, the accuracy drops quickly. Theoretically, our observation (e.g., the oscillation trends of approach and departure behaviors) should be independent of the number of tags in the system. However, due to the inherent characteristics of RFID protocols (ALOHA mechanism), when there is a large number of tags coexisting, the samples collected from each tag per second is reduced, which is also proved by the red line in Fig. 20. Under-sampling results that the tag signals can not capture the whole hand movement efficiently, and hence a decrease of the accuracy. Hence, we envision two solutions to solve this problem. First, according to the priority, we can filter out (choose not to read) some of the tags that are not desired. Second, the user can slow down his movement to guarantee sufficient samples of each tag.

6.2.8 Display Mode

We also examine the performance of detection under two display modes, horizontal and vertical mode, each for 50 times. Other settings are consistent with the experiments aforementioned. We find that APID performs well in both modes and the accuracy is 94 and 92 percent respectively.

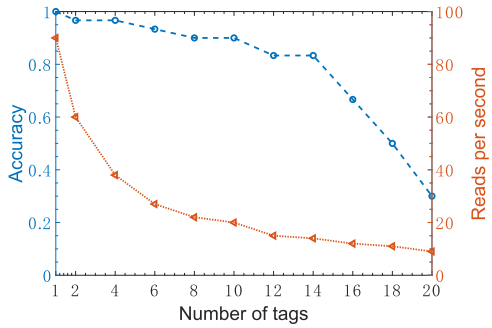

Fig. 20. The number of tags versus accuracy.

The results demonstrate that APID can achieve a high estimation accuracy in average, i.e., 93 percent.

6.3 Accuracy of Multi-object Scenario

We then exam the detection accuracy of APID in multi-object scenario. Experiments in this section focus on answering two questions. First, when multiple tags exist in the picking area, can APID successfully differentiate their signals? Second, when the deployment among objects changes, can APID still yield good performance?

6.3.1 Accuracy of EPC Decoding

To detect the real approach target of the user, the first step is to correctly separate EPC signals of different tags. In this part, we evaluate the effectiveness of our EPC decoder module. As mentioned in Section 5.1, when there is no movement around the tags, the HL-interval of each tag is stable and distinguishable. Thus, we collect signals from 5 Alien tags in a stable environment and distinguish them using their HL-intervals. We treat the labels deduced by HL-invervals as the ground truth, and compare them with the output of our decoder. We plot 300 results of HL-intervals for each tag in Fig. 21a, the values in different colors are labeled by the results derived from our decoder. From the results, we can obviously determine that there are only 4 errors (for Tag 4) among the overall 1500 tests. The accuracy of our EPC decoder is 98.7 percent+, as shown in Fig. 21b.

6.3.2 Accuracy versus Relative location

It is obvious that when a number of tags are closer to each other, the influence from an approach gesture to them is more similar. In addition, when the tags are within different radiation region of the reader antenna, the incident energy would be various. Thus, in this part, we investigate the impact of the relative location among tags on the detection accuracy. As shown in Fig. 22a, we put two tagged objects on the table, one of them always locates at the center of the reader's radiation region. The other tag locates at different positions towards four directions. Note that the reader's radiation region illustrated in Fig. 22a is simplified and idealized. The real radiation region would be more irregular and larger. Then we invite the volunteers to approach them respectively, 50 times for each. Fig. 22b shows the accuracy of four cases. We observe that for case A, the minimum accuracy, i.e., 88 percent, is achieved when the hand approaches Tag 2. We envision the reason is that when the volunteer approaches tag 2, the hand also moves above tag

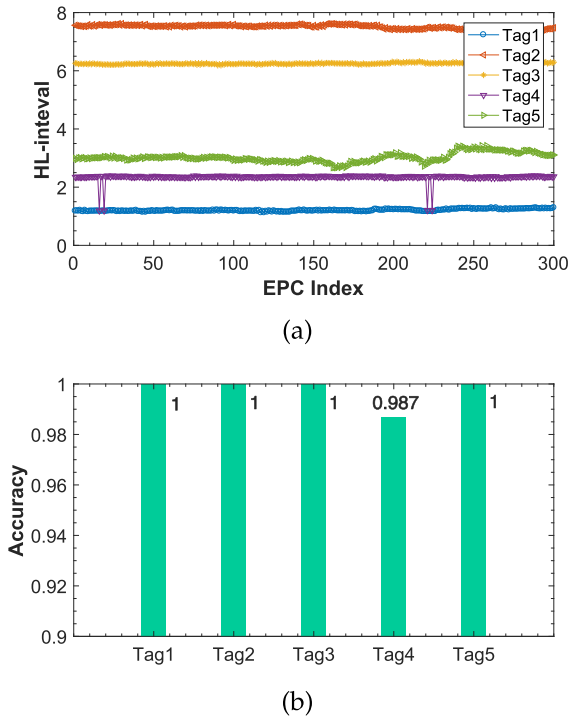

Fig. 21. (a) HL-intervals of different tags labeled by the results of our EPC decoder. (b) Accuracy of the decoder.

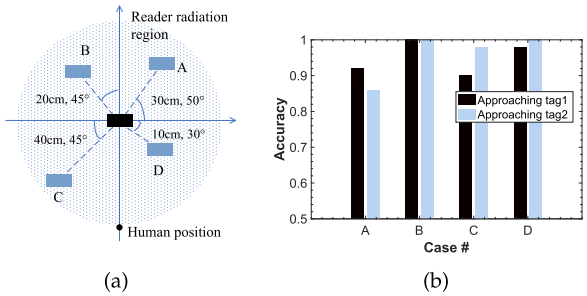

Fig. 22. (a) Planform of the experimental settings. (b) Approach target detection accuracy under different deployments.

1, which makes the data collected from them hard to distinguish. However, for other cases, APID performs well, even if the two tags are very close (only 10 cm apart, in case D).

6.3.3 Accuracy versus Antenna Region

In this trial of experiments, we keep the two tags' in-between distance constant (i.e., 30 cm), and change their positions together to make them within different reader's radiation sub-regions, as shown in Fig. 23a. Let d represent the corresponding distance. In each distance, the volunteers are asked to approach to two tags respectively, by repeating it for 50 times. The result in Fig. 23b indicates that APID can identify the approach target in most cases precisely. The average accuracy reaches up to 95 percent.

6.3.4 Accuracy versus Multiple Tags

Under each deploy modes, we conduct two types of experiments to verify the approach target detection accuracy among multiple tags. We deploy ten tags in a line with 10 cm in between or scatter them at random locations while the minimum distance between any two tags is 5 cm. The 15 volunteers are invited to approach to each tagged object 30

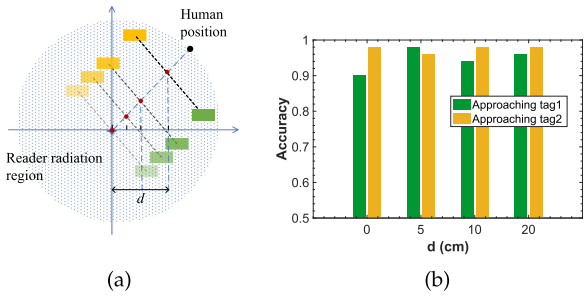

Fig. 23. (a) Planform of the experimental settings. (b) Approach target detection accuracy with different ds.

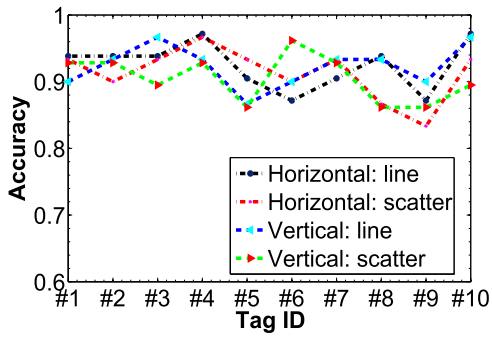

Fig. 24. Approach target detection accuracy in multi-object scenario under four deploy modes.

times, and we test if APID can correctly verify the target tag. The detection results are shown in Fig. 24. We can see that the accuracy of most detections are above 90 percent. The maximum number of errors occurs when the volunteer moves his hand to Tag #9 under horizontal mode with tags scattering at the table. In this case, APID considers it approaching to the adjacent tag (Tag #8). Overall, the average accuracy is about 91 percent.

7 Discussion and Limitation

In this section we discuss the limitations of APID.

Monitor Antenna Deployment. APID operates in the area covered by its monitor's antenna. To monitor the desired object on a table or a shelf, the monitor antenna can be deployed under the table or on the back of the shelf. The benefit of such deployment is that the monitor is close to the tags. The collected tag signals can be considered as coming from the reader-to-tag link, which can well reflect the signal variation modeled in Section 3.

Hand Moving Speed. Generally, the hand moving speed has little impact to the detection accuracy of APID. However, when enlarging the number of tags in the system, the readings of each tag every second will drop quickly. Undersampling will make the detection error-prone. Thus, APID prefers relatively slower movements.

Object Material. Current UHF RFID systems are designed to operate around the frequency of 900 MHz, with which the tags function well on the surface of most common materials, including wood, glass, paper, etc. However, RF transmission can be significantly affected by certain materials, such as metal and water, either completely reflecting an incident wave or absorbing it. Thus, APID may not work well for those materials.

8 Related Work

Prior works related to detecting approach or departure behaviors span a wide spectrum, mainly including the camera based, biological signal based, and wireless signal based schemes.

Camera based Schemas. Camera based schema is an important part of movement detection systems. These works often capture a sequence of images or videos through cameras, and build a movement indicator utilizing image processing and pattern recognition techniques [3], [4]. Camera based technique usually requires good lighting conditions of the environment. Other concerns, such as the privacy issue, also raise barrier for its application.

Biological Signal based Schemas. A wide corpus of research has concentrated on using specific equipment, such as the electromyography [15], [16] or electroencephalography electrodes [5], [17], to estimate human behaviors or movements. Zhao et al. [16] collect data about the EMG signals related with the given basic actions, and establish the correlation between them using classifiers or BP neural network technique. In addition, Lew et al. [5] detect self-paced upper limb movements from scalp electroencephalograph signals. The key limitation of biological signal based works is that they require attaching to or even embedding sensing devices into the human body, which is extremely inconvenient in daily life.

Wireless Signal based Schemas. Some works [11], [18], [19], [20], [21], [22], [23] have shown the feasibility of using wireless signals (such as WiFi, Z-wave, 60G radios) for motion or activity detection. Sigg et al. [24] propose to utilize RSS values of WiFi signals to recognize four activities, including walking, lying, crawling, and standing. They achieved an accuracy ($> 80\%$) in the activity recognition, and prove that RSS values can be used for recognizing these macro-movements. However, their work is not suitable to recognize the micro-movements such as moving hands [25] or fine-grained approach detection in a short range. WiTrack [18] tracks the 3D motion of a user using specially designed radar signals, i.e., Frequency Modulated Carrier Wave (FMCW) signals. RF-IDraw [26] attaches a UHF passive tag to the human's finger and leverages two readers and eight omni-directional antennas to track the tag trajectory, and hence infer human's writings. These techniques are either device-based [26], [27], [28] or requiring specially designed devices [18], [29] and complicated signal processing techniques before conducting the movement detection, limiting their application scope in practice. Compared to prior works, APID adopts new signal processing methods and schemes that are suitable for the Commercial-off-the-shelf (COTS) RFID (only several cents) transmission. It is fully compatible with the commercial RFID standard and can reuse RFID frastructures which may have already been deployed in many environments for object tracking purpose.

9 Conclusion

In this paper, we design and implement APID for near-proximity detection for hand approaching, without carrying special devices. APID is developed based on the observations of the influences of human hand movements to the vibration of backscattered tag signals, from both experiments and theoretical analysis. Experiments show that APID achieves high detection accuracy. Our initial assumption is that the reader has been deployed in applications for asset management. APID just supplements an extra functionality apart from identification, rather than serves as a dedicated approaching detection device.

Acknowledgments

This work is supported by the National Basic Research Program of China (973 Program) under Grant No.2015CB351705, NSFC Grant No. 61802299, 61872285, 61572396, 61772413, 61672424, National Key Research and Development Program of China under Grant 2016YFB0200902. Chen Qian was supported partially by US National Science Foundation Grants CNS-1717948 and CNS-1750704.

References

[1] L. Yang, Q. Lin, C. Duan, and Z. An, "Analog on-tag hashing: Towards selective reading as hash primitives in Gen2 RFID systems," in *Proc. 23rd Annu. Int. Conf. Mobile Comput. Netw.*, 2016, pp. 301–314.

[2] S. Pradhan, E. Chai, K. Sundaresan, L. Qiu, M. A. Khojastepour, and S. Rangarajan, "RIO: A pervasive RFID-based touch gesture interface," in *Proc. 23rd Annu. Int. Conf. Mobile Comput. Netw.*, 2017, pp. 261–274.

[3] Y. Wu, X. He, and T. Q. Nguyen, "Moving object detection with a freely moving camera via background motion subtraction," *IEEE Trans. Circuits Syst. Video Technol.*, vol. 27, no. 2, pp. 236–248, Feb. 2017.

[4] C.-C. Sun, Y.-H. Wang, and M.-H. Sheu, "Fast motion object detection algorithm using complementary depth image on an RGB-D camera," *IEEE Sensors J.*, vol. 17, no. 17, pp. 5728–5734, Sep. 2017.

[5] E. Lew, R. Chavarriaga, H. Zhang, M. Seeck, and J. Del Millan, "Self-paced Movement Intention Detection from Human Brain Signals: Invasive and Non-invasive EEG," in *Proc. IEEE Eng. Med. Biol. Soc.*, 2012, pp. 3280–3283.

[6] E. Wentink, S. Beijen, H. Hermens, J. Rietman, and P. Veltink, "Intention detection of gait initiation using EMG and kinematic data," *Gait Posture*, vol. 37, no. 2, pp. 223–228, 2013.

[7] C. Castellini and R. Koiva, "Using a high spatial resolution tactile sensor for intention detection," in *Proc. IEEE 13th Int. Conf. Rehabil. Robot.*, 2013, pp. 1–7.

[8] Y. Nakauchi, K. Noguchi, P. Somwong, T. Matsubara, and A. Namatame, "Vivid room: Human intention detection and activity support environment for ubiquitous autonomy," in *Proc. IEEE Int. Conf. Intell. Robots Syst.*, 2003, pp. 773–778.

[9] Wal-mart continues RFID technology expansion. May 1, 2007. [Online]. Available: https://corporate.walmart.com/_news_/news-archive/2007/05/01/wal-mart-continues-rfid-technology-expansion

[10] M. Buettner and D. Wetherall, "A Gen 2 RFID monitor based on the USRP," *ACM SIGCOMM Comput. Commun. Rev.*, vol. 40, no. 3, pp. 41–47, 2010.

[11] L. Shangguan, Z. Yang, A. X. Liu, Z. Zhou, and Y. Liu, "STPP: spatial-temporal phase profiling-based method for relative RFID tag localization," in *IEEE/ACM Trans. Netw.*, vol. 25, no. 1, pp. 596–609, 2017.

[12] GS1 EPCglobal Inc., *Specification for RFID Air Interface EPC: Radio-Frequency Identity Protocols Class-1 Generation-2 UHF RFID Protocol for Communications at 860 MHz-960 MHz*, 2008.

[13] H. Ding, H. Jinsong, L. Shangguan, W. Xi, Z. Jiang, Z. Yang, Z. Zhou, P. Yang, and J. Zhao, "A platform for free-weight exercise monitoring with RFIDs," *IEEE Trans. Mobile Comput.*, vol. 16, no. 12, pp. 3279–3293, Dec. 2017.

[14] B. Danev, D. Zanetti, and S. Capkun, "On physical-layer identification of wireless devices," *ACM Comput. Surv.*, vol. 45, 2012, Art. no. 6.

[15] K. H. Ha, H. A. Varol, and M. Goldfarb, "Volitional control of a prosthetic knee using surface electromyography," *IEEE Trans. Biomed. Eng.*, vol. 58, no. 1, pp. 144–151, Jan. 2011.

[16] H. Zhao and B. Wang, "Configuration of the mckibben muscles and action intention detection for an artificial assistant suit," *Int. J. Adv. Robot. Syst.*, vol. 9, no. 3, pp. 74–79, 2012.

[17] J. Ibáñez, J. Serrano, M. del Castillo, J. Gallego, and E. Rocon, "Online detector of movement intention based on EEG-application in tremor patients," *Biomed. Signal Process. Control*, vol. 8, no. 6, pp. 822–829, 2013.
[18] F. Adib, Z. Kabelac, D. Katabi, and R. C. Miller, "3D tracking via body radio reflections," in *Proc. 11th USENIX Conf. Netw. Syst. Des. Implementation*, 2014, pp. 317–329.
[19] F. Adib and D. Katabi, "See through walls with WiFi," in *Proc. ACM SIGCOMM Conf.*, 2013, pp. 75–86.
[20] H. Ding, J. Han, A. X. Liu, W. Xi, J. Zhao, P. Yang, and J. Zhao, "Counting human objects using backscattered radio frequency signal," *IEEE Trans. Mobile Comput.*, vol. 18, no. 5, pp. 1054–1067, May 2019.
[21] J. Han, H. Ding, C. Qian, D. Ma, W. Xi, Z. Wang, Z. Jiang, and L. Shangguan, "CBID: A customer behavior identification system using passive tags," in *Proc. IEEE 22nd Int. Conf. Netw. Protocols*, 2014, pp. 47–58.
[22] Q. Pu, S. Gupta, S. Gollakota, and S. Patel, "Whole-home gesture recognition using wireless signals," in *Proc. 19th Annu. Int. Conf. Mobile Comput. Netw.*, 2013, pp. 27–38.
[23] L. Shangguan, Z. Zhou, and K. Jamieson, "Enabling gesture-based interactions with objects," in *Proc. 15th Annu. Int. Conf. Mobile Syst. Appl. Serv.*, 2017, pp. 239–251.
[24] S. Sigg, M. Scholz, S. Shi, Y. Ji, and M. Beigl, "RF-sensing of activities from non-cooperative subjects in device-free recognition systems using ambient and local signals," *IEEE Trans. Mobile Comput.*, vol. 13, no. 4, pp. 907–920, Apr. 2014.
[25] K. Ali, A. X. Liu, W. Wang, and M. Shahzad, "Keystroke recognition using WiFi signals," in *Proc. 21st Annu. Int. Conf. Mobile Comput. Netw.*, 2015, pp. 90–102.
[26] J. Wang, D. Vasisht, and D. Katabi, "RF-IDraw: Virtual touch screen in the air using RF signals," in *Proc. ACM Conf. SIGCOMM*, 2014, pp. 235–246.
[27] P. Asadzadeh, K. Lars, and T. Egemen, "Gesture recognition using RFID technology," *Pers. Ubiquitous Comput.*, vol. 16, no. 3, pp. 225–234, 2012.
[28] K. Bouchard, B. Abdenour, and B. Bruno, "Gesture recognition in smart home using passive RFID technology," in *Proc. 7th Int. Conf. PErvasive Technol. Related Assistive Environments*, 2014, Art. no. 12.
[29] B. Kellogg, T. Vamsi, and G. Shyamnath, "Bringing gesture recognition to all devices," in *Proc. 11th USENIX Conf. Netw. Syst. Des. Implementation*, 2014, pp. 303–316.
[30] L. Xie, C. Wang, A. X. Liu, J. Sun, and S. Lu, "Multi-touch in the air: concurrent micromovement recognition using RF signals," *IEEE/ACM Trans. Netw.*, vol. 26, no. 1, pp. 231–244, 2018.
[31] L. Yang, Y. Chen, X.-Y. Li, C. Xiao, M. Li, and Y. L,, "Tagoram: real-time tracking of mobile RFID tags to high precision using COTS devices," in *Proc. 20th. Annu. Int. Conf. Mobile Comput. Netw.*, 2014, pp. 237–248.
[32] Y. Liu and Z. Li, "aLeak: privacy leakage through context-free wearable side-channel," in *Proc. IEEE Conf. Comput. Commun.*, 2018, pp. 1–9.

Han Ding received the PhD degree in computer science and technology from Xi'an Jiaotong University, in 2017. She is currently an assistant professor in Xi'an Jiaotong University. Her research interests focus on RFID system and smart sensing.

Chen Qian received the PhD degree from the University of Texas at Austin, in 2013. He is now an assistant professor with the Department of Computer Science and Engineering, University of California at Santa Cruz. His research interests include computer networking, Internet of Things, and network security. He received the NSF CAREER Award in 2018. He is a member of the IEEE and ACM.

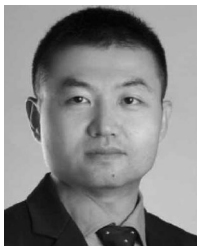

Jinsong Han received the PhD degree in computer science from the Hong Kong University of Science and Technology, in 2007. He is now a professor in the Institute of Cyberspace Research, College of Computer Science and Technology, Zhejiang University. He is a senior member of the ACM and IEEE. His research interests focus on mobile computing, RFID, and wireless network.

Jian Xiao received the BS degree in electronic engineering from the Chengdu University of Technology, China, in 1997 and the PhD degree from Lanzhou University, China, in 2008. He became a research assistant with Chang'an University, in June 2008. He is currently an associate professor with Chang'an University. His research interests include signal processing, artificial intelligence applications, pattern recognition, and computer vision.

Xingjun Zhang received the PhD degree in computer architecture from Xi'an Jiaotong University, China, in 2003. From 1999 to 2005, he was a lecturer and associate professor with the Department of Computer Science & Technology, Xi'an Jiaotong University. From Feb. 2006 to Jan. 2009, he was a research fellow with the Department of Electronic Engineering, Aston University, United Kingdom. He was an associate professor during 2009-2013 with the Department of Computer Science & Engineering, Xi'an Jiaotong University, where he has been a full professor from 2014. His interests include high performance computer architecture, high performance computing, big data storage system, and computer networks. He is a member of the IEEE.

Ge Wang received the BS degree from Xi'an Technological University, in 2013. She is working toward the PhD degree at Xi'an Jiaotong University. She is currently a visiting student at the University of California, Santa Cruz. Her research interests include wireless sensor network, RFID, and mobile computing. She is a student member of the IEEE.

Wei Xi received the PhD degree in computer science and technology from Xi'an Jiaotong University, in 2014. He is now an associate professor at Xi'an Jiaotong University. He is a member of the CCF, ACM, and IEEE. His research interests focus on wireless networks, smart sensing, and mobile computing.

Jizhong Zhao received the PhD degree in computer science and technology from Xi'an Jiaotong University, in 2001. He is now a professor at Xi'an Jiaotong University. He is a member of the CCF, ACM, and IEEE. His research interests focus on computer software, pervasive computing, distributed systems, and network security.